

# On the dynamics of the satellite galaxies in NGC 5044

Andreas Faltenbacher and William G. Mathews

*UCO/Lick Observatory, University of California at Santa Cruz, 1156 High Street, Santa Cruz, CA 95064, USA*

12 June 2018

## ABSTRACT

The NGC 5044 galaxy group is dominated by a luminous elliptical galaxy which is surrounded by  $\sim 160$  dwarf satellites. The projected number density profile of this dwarf population deviates within  $\sim 1/3$  of the virial radius from a projected NFW-profile, which is assumed to approximate the underlying total matter distribution. By means of a semi-analytic model we demonstrate that the interplay between gravitation, dynamical friction and tidal mass loss and destruction can explain the observed number density profile. We use only two parameters in our models: the total to stellar mass fraction of the satellite halos and the disruption efficiency. The disruption efficiency is expressed by a minimum radius. If the tidal radius of a galaxy (halo) falls below this radius it is assumed to become unobservable. The preferred parameters are an initial total to stellar mass fraction of  $\sim 20$  and a disruption radius of 4 kpc. In that model about 20 per cent of all the satellites are totally disrupted on their orbits within the group environment. Dynamical friction is less important in shaping the inner slope of the number density profile since the reduction in mass by tidal forces lowers the impact of the friction term. The main destruction mechanism is tide. In the preferred model the total B-band luminosity of all disrupted galaxies is about twice the observed luminosity of the central elliptical galaxy, indicating that a significant fraction of stars are scattered into the intragroup medium. Dwarf galaxy satellites closer to the centre of the NGC 5044 group may exhibit optical evidence of partial tidal disruption. If dynamical friction forces the satellite to merge with the central elliptical, the angular momentum of the satellite tends to be removed at the apo-centre passage. Afterwards the satellite drops radially towards the centre.

**Key words:** methods: numerical - galaxies: clusters: general - galaxies: dwarf - dark matter.

## 1 INTRODUCTION

It is generally accepted that the galaxy distribution in rich clusters of galaxies closely follows the dark matter distribution. In other words the number density of galaxies observed in clusters is well described by a Navarro, Frenk and White profile (Navarro et al. 1997). This behaviour is established by observations (see e.g. Carlberg et al. 1997; Biviano & Girardi 2003; Lin et al. 2004) as well as theoretical investigations (e.g. Gao et al. 2004; Kravtsov et al. 2004; Diaferio et al. 2001; Springel et al. 2001). In contradiction to these outcomes the number density profile of the galaxies in the NGC 5044 group shows a flattening towards the centre, which is not in agreement with the standard NFW profile (Mathews et al. 2004). The NGC 5044 group of galaxies resembles closely the properties of fossil groups (Ponman et al. 1994; Jones et al. 2000, 2003). The central elliptical galaxy in NGC 5044, with luminosity  $L_B = 4.5 \times 10^{10} L_{B\odot}$  is surrounded by  $\sim 160$  known dwarf satellites (Ferguson & Sandage 1990; Cellone & Buzzoni 2005). At a

distance of 33 Mpc (e.g. Tonry et al. 2001) the absolute magnitudes of the non-central galaxies range from  $M_B = -19$  to  $-13$ , i.e.  $2 \times 10^7 \lesssim L_B \lesssim 9 \times 10^9 L_{B\odot}$ . About 80 per cent of the group members appear to be spheroidal or dE galaxies.

The basic differences between the dark matter substructure (subhalo) distribution and the smoothly distributed component of cosmic matter assemblies is that substructures lose mass due to tidal forces and are affected by dynamical friction, whereas these two mechanisms have no impact on the smooth component. Both of these mechanisms can cause differences between the substructure distribution and the smoothly distributed matter component in groups and clusters of galaxies. Thus it is noteworthy that the galaxy number density profiles in rich clusters are in good agreement with the smooth density distribution. Dynamical friction and tidal mass loss seem to balance each other. Both mechanisms acting at the same time result in a distribution of the substructures which resembles the underlying smooth distribution. However, the radial number

density profile of satellite galaxies in the NGC 5044 group does not follow the underlying matter distribution. We estimate the expected radial distribution of galaxies in NGC 5044 by following the orbits in the time dependent potential well of the hosting halo. Since the masses of the dark halos that initially surround the stellar component of the satellites are not known well, we treat their *total to stellar mass ratio* ( $f_* = M_{tot}/M_*$ ) as a parameter in our computations. A second parameter which goes into the integration of the orbits is the *disruption radius*  $R_{dis}$ . Satellite halos that are truncated by tides down to this radius are assumed to reduce below the luminosity limit of the observations. We will show that the number density profile of the NGC 5044 galaxy population can be explained by the action of dynamical friction and tidal forces if total disruption of galaxies is allowed. When tidal disruption is considered it is no longer necessary to assume, as Mathews et al. (2004) have done, that the radial number density profile of satellite galaxies in NGC 5044 group requires an inherent deficiency of dwarf satellite galaxies at high redshifts. The tidally stripped stars may affect the intragroup medium, in particular the abundance of heavy elements (e.g. Zaritsky et al. 2004).

This paper is organised as follows. § 2 focuses on the integration of the galaxy orbits within the time dependent potential well of the hosting halo. In § 3 the number density profiles of the resulting satellite distribution at  $z = 0$  for different sets of parameters are discussed. § 4 investigates in detail the impact of dynamical friction versus tidal disruption. § 5 summarises the results obtained.

## 2 DYNAMICAL MODEL FOR NGC 5044

The model discussed here is a derivative of the model presented by Mathews et al. (2004). Very recently Zentner et al. (2005) demonstrated that this kind of semi-analytical model shows good agreement with state of the art N-body simulations. Similar approaches have been used for a variety of scientific goals, see e.g. Bullock et al. (2000, 2001); Zentner & Bullock (2003); Koushiappas et al. (2004); Taylor & Babul (2001, 2004); Islam et al. (2003); van den Bosch et al. (2005). The local space density of satellite galaxies is assumed to be proportional to that of the total gravitating matter, as if a fixed fraction of baryons formed into low-luminosity galaxies at a very early time. Thus the number of galaxies that have entered the virial radius of the host halo at a given time is proportional to the total amount of mass accreted at that time. Host and satellite halos are modelled according to findings of Wechsler et al. (2002). A random B-band luminosity is assigned to every satellite galaxy in such a way, that their luminosity distribution matches the distribution observed in NGC 5044. After a galaxy has entered the virial radius of the NGC 5044 group for the first time, its orbit is followed in the growing potential well of the host. The integration scheme takes dynamical friction and tidal mass loss into account. Satellites are assumed to be lost if their tidal radius falls below a certain radius. For simplicity we assume that all stars are formed at redshift  $z_* = 7$  (we also employed  $z_* = 3$  and 11, which does not change the overall picture). Dark matter halos formed at that epoch have central densities comparable to that of the stellar densities observed.

The underlying cosmology is the presently favoured concordance model with  $\Omega_m = 0.3$ ,  $\Omega_\Lambda = 0.7$ , a Hubble constant of  $70 \text{ km s}^{-1} \text{ Mpc}^{-1}$  and a normalisation of the power spectrum of  $\sigma_8 = 0.9$ .

### 2.1 Modelling the host halo

Following the analysis of Wechsler et al. (2002) the mass growth of the hosting halo can be described by

$$M_v(z) = M_{v,0} e^{-2a_f z} \quad (1)$$

where  $a_f = 1/(1+z_f)$  defines the halo formation time. The expansion factor  $a_f$  at the time of formation for NGC 5044 can be estimated by

$$c_{vir} = \frac{c_1 a_0}{a_f} . \quad (2)$$

If at present time  $a_0 = 1$  a concentration of  $c_{vir} = 11.1$  is assumed and  $c_1$  is set to 5.125 (Zentner et al. 2005) the expansion factor at formation turns out to be 0.46 which translates into a formation redshift of  $z_f = 1.2$ . Knowing the evolution of mass (Eq. 1) and concentration (Eq. 2) the virial radius at that redshift can be determined by the following formula.

$$r_{vir} = \left( \frac{3M(a)}{4\pi} \frac{1}{\Delta(a)\rho_c(a)} \right)^{1/3} \quad (3)$$

where  $\Delta(a)$  is a outcome of the spherical collapse approximation (see Eke et al. 1998; Bryan & Norman 1998). It gives the virialised overdensity with respect to the critical density  $\rho_c(a)$  at that epoch.  $M(a)$  is the time dependent mass specified in Eq. 1. With the above recipe the dark matter profile and the gravitational potential of the host can be computed for any radius and redshift. The orbits of the satellite halos are computed within this potential well.

### 2.2 Initial galaxy properties

We assume that all satellite galaxies form at the same early redshift  $z_*$  and that their space density is proportional to that of the dark matter. Thus the satellites enter the host halo at the same rate as the dark matter. With this simple model the host mass  $M_{v,i}$  when the *i*th satellite first entered the virial radius of the host can be found from

$$M_{v,i} = \mathcal{R}_M M_{v,0} \quad (4)$$

where  $0 \leq \mathcal{R}_M \leq 1$  is a random number and  $M_{v,0} = 3.9 \times 10^{13} M_\odot$  is the current virial mass of the NGC 5044 group. The virial mass of the host at entry of the *i*th satellite can be translated into a redshift  $z_i$  via Eq. 1 and a virial radius  $r_{v,i}$  by Eq. 3. The velocity of the galaxy at the virial radius is the free-fall velocity from the turnaround radius  $r_t = 2r_{v,i}$ .

$$u_{v,i} = (GM_{v,i}/r_{v,i})^{1/2} \quad (5)$$

The stellar mass of the *i*th galaxy is

$$m_{*,i} = \Upsilon_B L_{B,i} . \quad (6)$$

Here the galactic luminosity is randomly selected from the power law part of the Schechter luminosity function  $dN/dL_B \propto L_B^{-1.2}$  (which is satisfied in NGC 5044):

$$L_{B,i} = [L_1^{-0.2} - \mathcal{R}_L (L_1^{-0.2} - L_2^{-0.2})]^{-5} , \quad (7)$$

with  $L_1 = 2 \times 10^7 L_{B\odot}$  and  $L_2 = 9 \times 10^9 L_{B\odot}$  and  $\mathcal{R}_L$  is another random ( $0 \leq \mathcal{R}_M \leq 1$ ). For the stellar mass to light ratio  $\Upsilon_B$  in Eq. 6 we adopt

$$\Upsilon_B = 0.71 \times L^{0.1} \quad (8)$$

as discussed by Trujillo et al. (2004). We assume that the galaxies form in isolation. Thus it is reasonable to embed them into a dark matter halo. Since the ratio between total and stellar matter in isolated dwarf galaxies is not well determined, we introduce a parameter  $f_* = M_{tot}/M_*$  which allows us to vary the star formation efficiency. The total mass of the satellite including the dark matter halo is then given by

$$m_{tot,i} = f_* \Upsilon_B L_{B,i}. \quad (9)$$

The density profile of all matter components - dark, stellar and gaseous - is assumed to follow a NFW-profile which is in agreement with recent studies by Colín et al. (2004) who showed that the density profiles of dwarf (N-body) halos are well fitted by NFW-profiles. The concentration of each satellite halo accreting at redshift  $z_i$  is computed by means of Eq. 2. For this purpose  $a_0$  has to be interpreted as the expansion factor at arrival ( $a_0 = 1/(1+z_i)$ ) and  $a_f$  corresponds to the formation redshift of the halo  $a_f = 1/(1+z_*)$ . As mentioned above, the choice of different formation redshifts  $z_* = 3, 7, 11$ , has marginal influence on the results. Subsequently, we assume  $z_* = 7$  for the global formation redshift of the satellite halos. This simplifications do not pay tribute to the dissipative baryonic processes, like radiation or adiabatic contraction (see e.g. Gnedin et al. 2004). Due to these processes the central parts of the satellite halos might be more tightly bound and the total tidal destruction might become more difficult. This shortcoming can be compensated by the variation of the the second parameter introduced here, the *disruption radius*  $R_{dis}$ . If the tidal forces manage to strip the outer matter shells down to this radius, the satellite galaxy is assumed to vanish, i.e. fall below optical observability. We adjust this parameter to reach agreement with the global satellite distribution observed in NGC 5044, without tackling the complex processes close to the halo centre.

### 2.3 Integration of the orbits

We integrate the orbits of each satellite galaxy starting at the virial radius when the satellite first enters the virialised halo of the host. The absolute value of the initial velocity is computed under the assumption that the satellite has experienced free-fall from twice the virial radius, Eq. 5. The absolute value of the velocity is distributed to a radial and a tangential component. The tangential component is assigned in accordance with the results by Tormen (1997) (see also Zentner et al. 2005). He gives a distribution of circularity  $\epsilon = J/J_c$  of dark matter particles at the virial radius. Here  $J$  is the specific angular momentum of the dark matter particle and  $J_c$  is the maximum possible specific angular momentum of bound particles at that radius.  $\epsilon = 0$  or  $1$  indicates radial or circular orbits, respectively. Based on these results we model (see Mathews et al. 2004) the probability density for circularity  $p' = dp/d\epsilon$  with a third order polynomial, subject to the constraints that  $p'(0) = p'(1) = 0$  and

normalised so the integral of  $p'(\epsilon)$  from 0 to 1 is unity. The resulting distribution is

$$p'(\epsilon) = a\epsilon^3 - (1.5a + 6)\epsilon^2 + (0.5a + 6)\epsilon \quad (10)$$

where

$$a = 60(1 - 2\langle\epsilon\rangle). \quad (11)$$

The results of Tormen suggest that  $\langle\epsilon\rangle \approx 0.5$ , for which  $p'(\epsilon)$  becomes a symmetric quadratic.

The orbits of the satellites are found by solving

$$\frac{d\mathbf{r}}{dt} = \mathbf{u} \quad \text{and} \quad \frac{d\mathbf{u}}{dt} = -\frac{GM(r)}{r^2} \frac{\mathbf{r}}{r} + \left(\frac{d\mathbf{u}}{dt}\right)_{df}, \quad (12)$$

where  $M(r)$  is the NFW mass within the radius  $r$  of the host halo at that time. Orbits are computed from redshift  $z_i$  (redshift of entry) to  $z = 0$ . The deceleration by dynamical friction (Chandrasekhar 1943; Colpi et al. 1999) can be described by

$$\left(\frac{d\mathbf{u}}{dt}\right)_{df} = -\mathbf{u} 4\pi \ln \Lambda G^2 m \rho u^{-3} [\text{erf}(X) - \frac{2}{\pi^{1/2}} X e^{-X^2}]. \quad (13)$$

Here  $\rho(r, t)$  is the local density of the host halo,  $u = |\mathbf{u}|$  is the velocity of the satellite,  $X = u/(\sqrt{2}\sigma)$  and  $\sigma(r, t)$  is the mean velocity dispersion in NGC 5044. We assume that the total dispersion can be approximated by the cold dark matter dispersion presented by Hoesft et al. (2004) (see also Mathews et al. 2004). We choose  $\ln \Lambda = 3$  as suggested by Zhang et al. (2002) which is the point mass approximation. This approximation is justified by the very efficient tidal mass stripping which effectively truncates the radius of the satellite halo.

The tidal truncation radius is estimated by the Jacobi limit (see Binney & Tremaine 1987; Hayashi et al. 2004).

$$r_J = \left(\frac{m_{tot,i}}{3M(< D)}\right)^{1/3} D \quad (14)$$

Here  $D$  is the distance of the satellite to the centre of the group,  $M(< D)$  is the mass of the host within  $D$  and  $m_{tot,i}$  is the current mass of the halo. If the resulting truncation radius  $r_J$  is smaller than the current radius of the satellite halo, then the truncation radius is assumed to be the current halo radius and all the matter outside of  $r_J$  is stripped instantaneously. In our model a minimum disruption radius  $R_{dis}$  is introduced. If the truncation radius falls below this radius the satellite's luminosity is assumed to fall below observability. We will show models for  $R_{dis} = 0, 2, 4$  and  $6$  kpc, respectively. For  $R_{dis} = 0$  all the satellites survive. For comparison the effective radius of the lowest luminosity dwarfs in NGC 5044 is approximately  $4$  kpc. We do not allow a change of the density or velocity profile of the satellite halo following the truncation. Kazantzidis et al. (2004) have shown that a cuspy density profile remains after mass is lost by tidal forces. However, tidal heating (see e.g. Gnedin 2003) may reduce the central density and therefore reduce the mass contained within the truncation radius. In fact by means of N-body simulations Hayashi et al. (2004) and Kravtsov et al. (2004) have shown that some mass is lost even within the tidal radius of sub-halos orbiting in the potential well of a host halo. Hayashi et al. (2004) compare different estimators for the truncation radius, concluding that the Jacobi limit most accurately estimates this additional tidal mass loss.

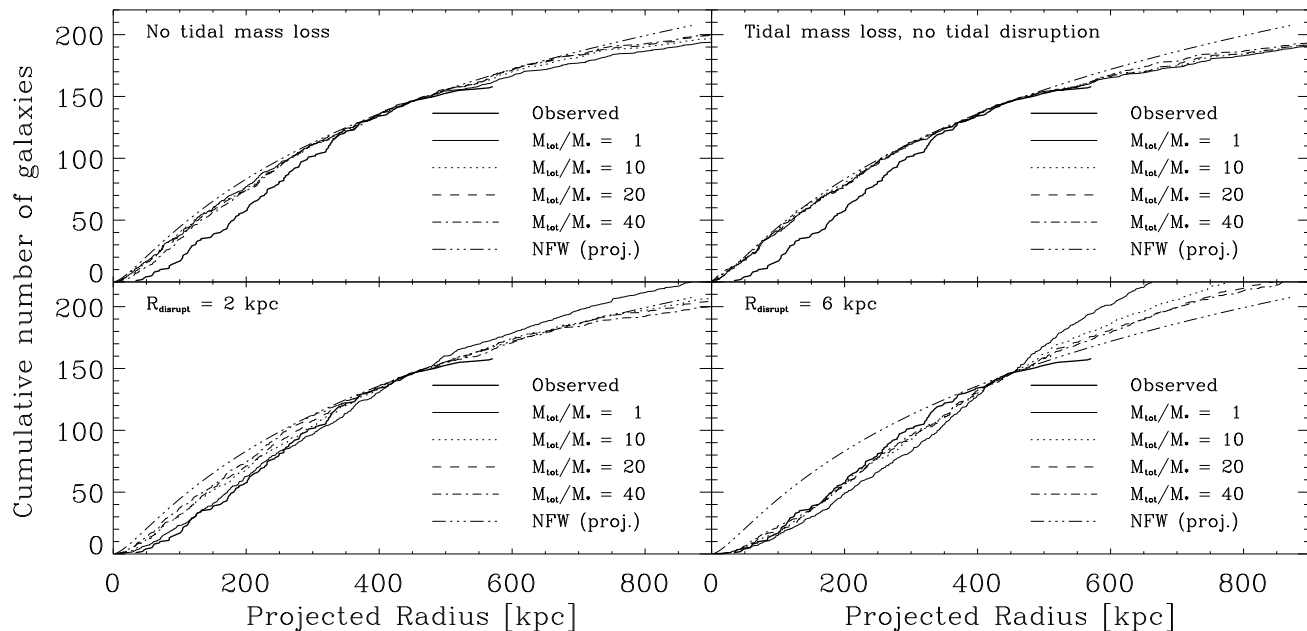


**Figure 1.** Comparison of the observed galaxy distribution in NGC 5044 (thick solid line) with the different model profiles. The various thin lines indicate alternate mass ratios between the total mass of the halo and the stellar component as indicated by the legend within each plot. The upper left-hand panel shows the resulting profiles if tidal mass loss is not taken into account. In the upper right panel tidal mass loss is tracked but the halos never are assumed to be disrupted. The lower panels depict the profiles if halo disruption is implemented. The disruption radii are assumed to be on left- and right-hand side 2 kpc and 6 kpc, respectively.

Therefore we apply the Jacoby limit. Nevertheless, due to the dense baryonic cores, more mass may be retained than estimated from pure N-body investigations. We assume that the net trend of the different processes can be represented by an appropriate choice of the disruption radius  $R_{dis}$  that generates the final observed number distribution. Since the force exerted by dynamical friction is proportional to the mass squared, tidal mass loss strongly reduces the impact of dynamical friction.

### 3 NUMBER DENSITY PROFILES

In this section we present the resulting number density profiles for different sets of parameters. As mentioned above we use only two parameters, firstly the initial total to stellar mass ratio  $f_*$  to vary the contribution of the cold dark matter halo, secondly the disruption radius  $R_{dis}$  which modulates the destruction rate due to tidal forces. Fig. 1 shows the results for four different tidal disruption/destruction efficiencies.

The upper left panel displays the radial distribution resulting from dynamical friction without tidal mass loss. This scenario is rather unphysical since observations (e.g. Majewski et al. 2004; Rocha-Pinto et al. 2004) and N-body simulations (e.g. Diemand et al. 2004; Kravtsov et al. 2004; Nagai & Kravtsov 2005) have proven that tidal mass loss is significant. However it is interesting to note that the different masses of the satellite halos due to different  $f_*$ -values do not result in greatly different profiles. All profiles fall a little below the projected NFW-profile and are equally discrepant when compared to the observations. Dynamical

friction shifts the whole distribution inwards without seriously affecting the overall shape.

The upper panel on the right in Fig. 1 shows the resulting distribution if tidal mass loss is allowed but total tidal destruction is not allowed ( $R_{dis} = 0$ ). This prescription is similar to the treatment of the cluster galaxies in Gao et al. (2004). In agreement with their findings the galaxy number density profile follows closely the NFW-profile (at least within the  $\sim \frac{2}{3}$  of the virial radius). However the resulting profiles are not in agreement with observations of NGC 5044. This difference emphasises that the shallow potential wells of the faint dwarf galaxies in NGC 5044 must be considered. Observations addressing the dwarf populations in clusters of galaxies suggest that the dwarf galaxies can be strongly affected by tidal forces. According to Dahlén et al. (2004) and Lin et al. (2004) the decreasing dwarf-to-giant ratio with increasing surface density in clusters of galaxies indicates that the high density environments are hostile to dwarf galaxies.

The lower panels in Fig. 1 compare the the observed projected satellite distribution with model profiles for two different tidal destruction efficiencies,  $R_{dis} = 2$  and  $R_{dis} = 6$  kpc. In the lower left-hand panel only the distribution with  $f_* = 1$  matches the observed distribution below 450 kpc. But the strong increase above 450 kpc and the fact that a mass to light ratio of 1 entirely neglects the contribution of cold dark matter gives evidence against this particular model. The model profiles in the lower right-hand panel agree with the observation for  $f_* = 10, 20$  and  $40$  below radii of 450 kpc, but obviously exceed the data and the NFW profile for large radii. (It should be mentioned that the observed distribution is likely to be incomplete at large radii.) The census of

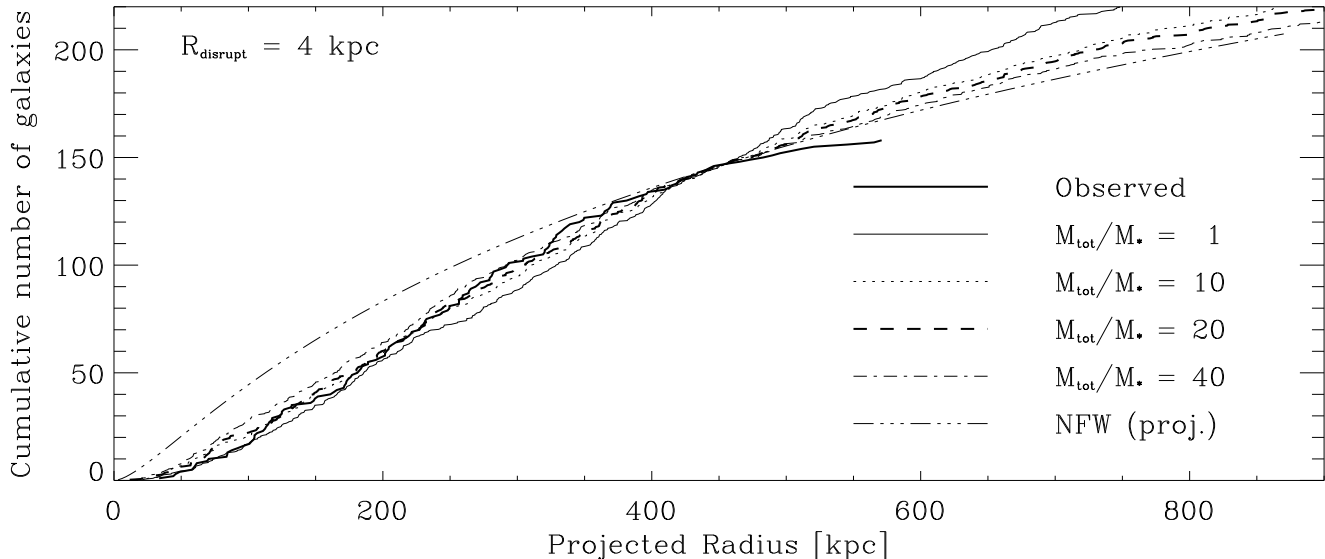


**Figure 2.** Comparison of the observed galaxy distribution in NGC 5044 (thick solid line) with the different model profiles for a disruption radius of 4 kpc. The various thin lines indicate alternate mass ratios between the total mass of the halo and the stellar component as indicated by the legend. The thick dashed line belonging to a stellar to total mass ratio of 20 marks the favoured model.

surviving satellite galaxies in Tab. 1 indicates that a large fraction of satellites ( $\sim 30$  per cent) have been destroyed.

Fig. 2 presents a model with disruption radius  $R_{dis} = 4$  kpc that matches the data for NGC 5044 very well. Interestingly this  $R_{dis}$  turns out to be equal to the effective radius of the faintest galaxies observed in NGC 5044, if the minimum B-band luminosity  $L_B = 2 \times 10^7 L_{B\odot}$  is transformed into an effective radius  $R_e$  using the relation given in De Rijcke et al. (2004). The total to stellar mass ratio which approximates the data best is  $f_* = 20$ , or perhaps a bit lower since choosing  $f_* = 10$  results in very a similar behaviour. Prada et al. (2003) have shown that the consideration of the dark matter halo of isolated galaxies leads to  $M_{tot}/L_B \approx 130$  for galaxies within the luminosity range of  $1 \times 10^{10} \lesssim L_B \lesssim 4 \times 10^{10} L_{B\odot}$  corresponding roughly to  $f_* = M_{tot}/M_* = 16$ . Therefore the chosen parameter set seems to be in good agreement with recent observations. As indicated by the bold line in Tab. 1, these parameters lead to a stellar loss rate of  $\sim 20$  per cent. The total luminosity of all these lost galaxies is  $9.4 \times 10^{10} L_{B\odot}$ . This luminosity is twice as high as the luminosity of the central elliptical galaxy in NGC 5044,  $L_B = 4.5 \times 10^{10} L_{B\odot}$ , but only  $\sim 35$  per cent of the total B-band luminosity in the group including all dwarf galaxies  $L_{B,d} \approx 13.7 \times 10^{10} L_{B\odot}$  (corrected for incompleteness, the corresponding B-band luminosity within  $r_{vir}$  in the best fitting model is  $L_{B,d} \approx 16.9 \times 10^{10} L_{B\odot}$ ) and galaxies disrupted in the model. Evidently, the missing stars are scattered in the intragroup medium (see e.g. Zaritsky et al. 2004; Sommer-Larsen et al. 2005).

We have shown the results for a uniform formation redshift of  $z_* = 7$ . Different formation redshifts result in different concentrations of the satellite halos and thus might affect the tidal stripping efficiency. Therefore we have redone the modelling with formation redshifts of  $z_* = 3$  and 11. The differences are marginal. We conclude this section by

$R_{dis}$	$M_{tot}/M_*$	$N_{cen}/N_{vir}$	$N_{fric}$	$N_{tid}$	$L_{B\odot}$
2	1	0.26	0	173	$6.4 \times 10^{10}$
2	10	0.10	0	63	$3.8 \times 10^{10}$
2	20	0.08	2	47	$4.9 \times 10^{10}$
2	40	0.06	8	31	$6.5 \times 10^{10}$
4	1	0.68	0	486	$2.4 \times 10^{11}$
4	10	0.25	0	170	$8.4 \times 10^{10}$
<b>4</b>	<b>20</b>	<b>0.21</b>	<b>3</b>	<b>137</b>	<b><math>9.4 \times 10^{10}</math></b>
4	40	0.18	7	110	$1.1 \times 10^{11}$
6	1	1.34	0	1075	$6.3 \times 10^{11}$
6	10	0.42	0	297	$1.5 \times 10^{11}$
6	20	0.32	3	219	$1.3 \times 10^{11}$
6	40	0.28	7	179	$1.4 \times 10^{11}$

**Table 1.** Survival rates. The first two columns display the disruption radius and total to stellar mass, respectively. The third column gives the fraction of galaxies that ended in the centre to the current number of galaxies within the virial radius. The following two columns list the number of galaxies that disappeared due to dynamical friction and tidal disruption. The last column shows the summed luminosity of all galaxies that have been destroyed. The bold face line indicates the favoured model.

repeating that the model parameters  $f_* = 20$ ,  $R_{dis} = 4$  kpc and  $z_* = 7$  match the data very well.

#### 4 DYNAMICAL FRICTION AND TIDAL MASS LOSS

In this section we show the orbital behaviour of three particular galaxies. These three cases are chosen to make some of the features discussed above more explicit. In Figs. 3, 4 and 5 we compare the behaviour of satellite halos having the same initial conditions with (solid and dashed lines) and

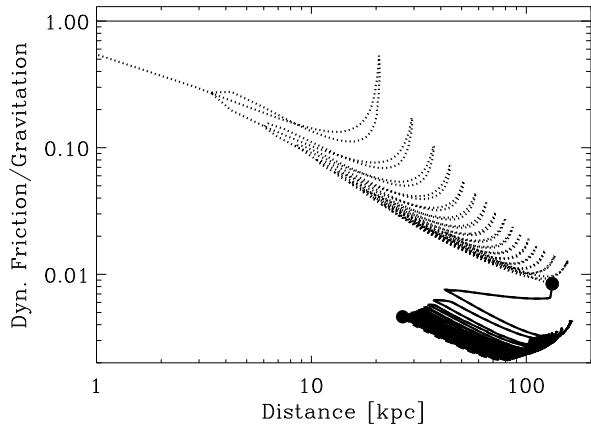


**Figure 3.** Trajectory of a model galaxy. The ratio of forces caused by dynamical friction and by gravitation is plotted versus the physical distance of the galaxy from the centre of the group. The large, right dot marks the first penetration of the galaxy through the virial radius. The dotted line represents the path of the galaxy if tidal mass loss is suppressed but retaining dynamical friction. The solid and dashed (almost totally hidden) lines show the path if tidal mass loss is also taken into account. The left dot marks the location where the galaxy is assumed to be tidally lost if a disruption radius of 4 kpc is applied. The dashed line follows the path of the galaxy till  $z = 0$  if the galaxy suffers no tidal destruction ( $R_{dis} = 0$ ). The solid horizontal line at the top separates the friction dominated area from the area where gravitation prevails.

without (dotted lines) tidal mass loss. The dashed lines indicate the orbits without tidal destruction, whereas the solid line ends (additionally marked by a second large dot) when the truncation radius falls below 4 kpc. In these figures the ratio of the forces due to dynamical friction and gravitation ( $F/G$ ) is plotted versus the distance of the satellite to the centre of the group. The horizontal line for  $F/G = 1$  indicates the threshold where dynamical friction equals the force exerted by gravitation. Once an orbit transgresses above this line, it is dominated by dynamical friction and the galaxy drops nearly radially toward the centre.

The large, right dot in Fig. 3 marks the first passage through the virial radius and therefore the beginning of integration. After orbiting once around the group centre the satellite moves farther outwards because its initial velocity was the free-fall velocity from twice the virial radius. The eccentricity of the orbit without tidal stripping (dotted line) changes from initially  $\epsilon \approx 0.6$  to a final value of  $\approx 0.7$ . Interestingly the contribution of friction to the total force shows a minimum for intermediate radii and rises again if the satellite moves further out. Dynamical friction is not negligible during the apo-centre passage. For small velocities  $F/G$  is roughly proportional to  $r/u$ , where  $r$  is the distance to the group centre and  $u$  is absolute values of the velocity. Frictional decay of the tangential velocity at apo-centre leads to more radial orbits, if tidal mass loss is not taken into account. Furthermore the computed orbit indicates that satellites can first transgress the  $F/G = 1$  line during their apo-centre passage. In that case all the angular momentum of the satellite is lost and it approaches the centre on a pure radial orbit. Such an orbit might be appropriate for a mas-

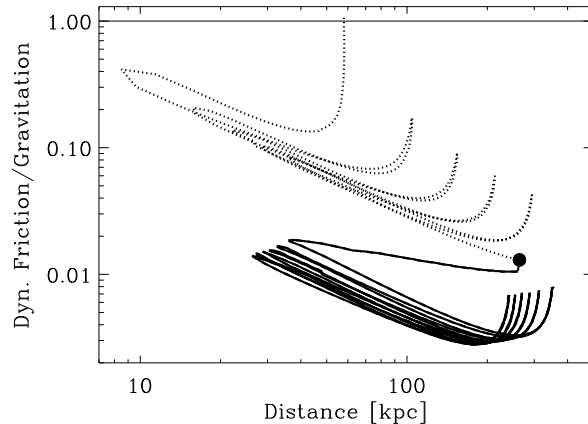


**Figure 4.** Trajectory of a model galaxy, the description is the same as in Fig. 3. The absence of the second black dot indicates that this halo is not destroyed by tidal forces when a disruption radius of 4 kpc is applied.

sive black hole that experiences dynamical friction without tidal losses. The eccentricity of the orbit with tidal stripping (solid/dashed line) stays  $\approx 0.6$  all the time. This is due to that fact that tidal stripping reduces the action of dynamical friction. Most of the mass is lost during the first infall, as can be inferred by the shallow slope till the first pericentre passage. The large, left dot indicates where the tidal destruction is assumed by our approach. Here  $R_{dis} = 4$  kpc was chosen. Fig. 3 shows that after  $\sim 10$  orbits the satellite is destroyed at a distance  $\sim 25$  kpc from the centre, which is quite close to the central elliptical galaxy.

The orbit shown in Fig. 4 has a similar behaviour, but differs from the previous orbit in that the satellite is not destroyed by tidal forces (no second large dot). Without tidal stripping and mass loss (dotted line) the satellite halo eventually falls toward the group centre as indicated by the final passage above the  $F/G = 1$  line. This catastrophic loss of angular momentum by dynamical friction occurs during an apo-centre passage. When all its orbital angular momentum is lost, the satellite approaches the centre on a radial orbit starting at  $\sim 60$  kpc from the centre. The eccentricity of the orbit without tidal stripping changes from  $\approx 0.8$  to  $\approx 0.7$ , whereas the orbit with tidal mass loss retains its initially eccentricity of  $\approx 0.8$ .

Fig. 5 is an example for a very radial orbit in which the eccentricity remains at  $\approx 0.9$  for all orbits, either with or without tidal mass loss. The large initial radius  $\sim 450$  kpc indicates that the satellite approaches rather late, that means the potential well of the hosting group is already very deep. The large, left dot marks the destruction during the first peri-centre passage, if tidal stripping and destruction are allowed ( $R_{dis} = 4$  kpc). For this particular case, which is rather extreme, the fast destruction seems reliable, since the satellite is falling from  $\sim 900$  kpc (twice the virial radius at epoch of entry) down to  $\sim 20$  kpc which is very close to the central elliptical galaxy.

The detailed analysis of the individual orbits clearly demonstrates that the influence of dynamical friction is largely reduced by tidal mass loss. The estimation of the tidal radius by the Jacobi limit and the instantaneous strip-

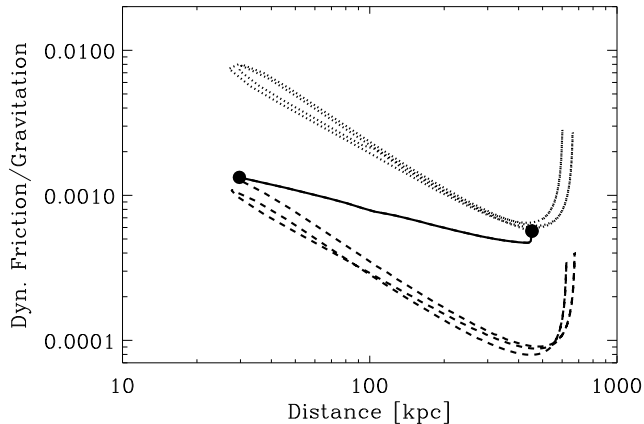


**Figure 5.** Trajectory of a model galaxy, the description is the same as in Fig. 3.

ping up to this radius lead to a rapid decrease of the halo mass during the first infall. The instantaneous stripping description might reduce the mass a bit to fast, but after very few orbits the Jacobi radius should be a good approximation. On subsequent orbits dynamical friction tends to push the halo closer to the centre which is accompanied by further tidal mass loss, since the tidal radius of the halo is proportional to its distance from the centre. The force exerted by dynamical friction is proportional to the halo mass squared, thus the loss of mass reduces the impact of friction further. In conclusion the dominant process for shaping the inner number density profile of groups like NGC 5044 is tidal disruption and/or destruction.

## 5 CONCLUSION

Using a simple model we find that the interplay between dynamical friction and tidal disruption can explain the shallow slope of the projected number density profiles of satellite galaxies of the fossil group NGC 5044. The strong deviation of observed satellite galaxies from NFW profiles is a result of the tidal disruption of the stellar cores of galaxies orbiting closer to the group centre. This feature may be more naturally explained in this manner than by assuming an absence of dwarf galaxies at high redshifts (Mathews et al. 2004). We use two parameters to model the observed dwarf galaxy distribution: the total to stellar mass ratio  $f_*$  and the disruption radius  $R_{dis}$ . With parameters  $f_* \approx 20$  and  $R_{dis} \approx 4$  kpc the model can match the observed projected radial number distribution in NGC 5044 very well.  $f_* \approx 20$  is in good agreement with the findings of Prada et al. (2003). They show that the  $M_{tot}/L_B$  of isolated galaxies with B-band luminosities of  $1 \times 10^{10} \lesssim L_B \lesssim 4 \times 10^{10} L_{B\odot}$  is in the range between 100 and 150. For  $f_* = 20$  we obtain  $M_{tot}/L_B \approx 160$ . If we use the  $R_e - L_B$  relation presented by De Rijcke et al. (2004) to compute the effective radius for our lowest luminosity model galaxies ( $L_B \approx 2 \times 10^7 L_{B\odot}$ ) we obtain  $R_e \approx 4$  kpc. Therefore, the global galaxy distribution in NGC 5044 seems to favour a destruction radius that is close to the minimal  $R_e$  of the group satellites.

We find that the total luminosity of the tidally dis-

rupted galaxies is about twice the luminosity of the central elliptical or  $\sim 35$  per cent of the total optical light of the group, allowing for incompleteness of identified satellite galaxies. This indicates that a large fraction of satellite stars are scattered into the intragroup medium by tidal forces. Using the near-infrared  $K$ -band properties of clusters Lin & Mohr (2004) estimate that a large fraction (50 per cent) of the total stellar luminosity is contributed by intracluster light. This fraction increases with cluster mass. Neill et al. (2005) searched the Fornax cluster for novae in between the galaxies and find that  $\sim 16 - 41$  per cent of the total cluster light comes from the intracluster stars. Dwarf galaxies orbiting close to the centre of groups like NGC 5044 may show morphological evidence of partial tidal destruction.

## ACKNOWLEDGEMENTS

The authors would like to thank the anonymous referee for his comments which helped to clarify the text. This work has been supported by NSF grant AST 00-98351 and NASA grant NAG5-13275 for which we are very grateful.

## REFERENCES

- Binney J., Tremaine S., 1987, Galactic dynamics. Princeton, NJ, Princeton University Press, 1987, 747p.
- Biviano A., Girardi M., 2003, ApJ, 585, 205
- Bryan G. L., Norman M. L., 1998, ApJ, 495, 80
- Bullock J. S., Kravtsov A. V., Weinberg D. H., 2000, ApJ, 539, 517
- Bullock J. S., Kravtsov A. V., Weinberg D. H., 2001, ApJ, 548, 33
- Carlberg R. G., Yee H. K. C., Ellingson E., 1997, ApJ, 478, 462
- Cellone S. A., Buzzoni A., 2005, MNRAS, 356, 41
- Chandrasekhar S., 1943, ApJ, 97, 255
- Colín P., Klypin A., Valenzuela O., Gottlöber S., 2004, ApJ, 612, 50
- Colpi M., Mayer L., Governato F., 1999, ApJ, 525, 720
- Dahlén T., Fransson C., Östlin G., Näslund M., 2004, MNRAS, 350, 253
- De Rijcke S., Michielsen D., Dejonghe H., Zeilinger W. W., Hau G. K. T., 2004, A&A, 438, 491
- Diaferio A., Kauffmann G., Balogh M. L., White S. D. M., Schade D., Ellingson E., 2001, MNRAS, 323, 999
- Diemand J., Moore B., Stadel J., 2004, MNRAS, 352, 535
- Eke V. R., Navarro J. F., Frenk C. S., 1998, ApJ, 503, 569
- Ferguson H. C., Sandage A., 1990, AJ, 100, 1
- Gao L., De Lucia G., White S. D. M., Jenkins A., 2004, MNRAS, 352, L1
- Gnedin O. Y., 2003, ApJ, 582, 141
- Gnedin O. Y., Kravtsov A. V., Klypin A. A., Nagai D., 2004, ApJ, 616, 16
- Hayashi E., Navarro J. F., Power C., Jenkins A., Frenk C. S., White S. D. M., Springel V., Stadel J., Quinn T. R., 2004, MNRAS, 355, 794
- Hoefl M., Mucket J. P., Gottlöber S., 2004, ApJ, 602, 162
- Islam R. R., Taylor J. E., Silk J., 2003, MNRAS, 340, 647

- Jones L. R., Ponman T. J., Forbes D. A., 2000, MNRAS, 312, 139
- Jones L. R., Ponman T. J., Horton A., Babul A., Ebeling H., Burke D. J., 2003, MNRAS, 343, 627
- Kazantzidis S., Mayer L., Mastropietro C., Diemand J., Stadel J., Moore B., 2004, ApJ, 608, 663
- Koushiappas S. M., Zentner A. R., Walker T. P., 2004, Phys. Rev. D, 69, 043501
- Kravtsov A. V., Gnedin O. Y., Klypin A. A., 2004, ApJ, 609, 482
- Lin Y., Mohr J. J., 2004, ApJ, 617, 879
- Lin Y., Mohr J. J., Stanford S. A., 2004, ApJ, 610, 745
- Majewski S. R., Ostheimer J. C., Rocha-Pinto H. J., Patterson R. J., Guhathakurta P., Reitzel D., 2004, ApJ, 615, 738
- Mathews W. G., Chomiuk L., Brighenti F., Buote D. A., 2004, ApJ, 616, 745
- Nagai D., Kravtsov A. V., 2005, ApJ, 618, 557
- Navarro J. F., Frenk C. S., White S. D. M., 1997, 490, 493
- Neill J. D., Shara M. M., Oegerle W. R., 2005, ApJ, 618, 692
- Ponman T. J., Allan D. J., Jones L. R., Merrifield M., McHardy I. M., Lehto H. J., Luppino G. A., 1994, Nature, 369, 462
- Prada F., Vitvitska M., Klypin A., Holtzman J. A., Schlegel D. J., Grebel E. K., Rix H.-W., Brinkmann J., McKay T. A., Csabai I., 2003, ApJ, 598, 260
- Rocha-Pinto H. J., Majewski S. R., Skrutskie M. F., Crane J. D., Patterson R. J., 2004, ApJ, 615, 732
- Sommer-Larsen J., Romeo A. D., Portinari L., 2005, MNRAS, 357, 478
- Springel V., White S. D. M., Tormen G., Kauffmann G., 2001, MNRAS, 328, 726
- Taylor J. E., Babul A., 2001, ApJ, 559, 716
- Taylor J. E., Babul A., 2004, MNRAS, 348, 811
- Tonry J. L., Dressler A., Blakeslee J. P., Ajhar E. A., Fletcher A. B., Luppino G. A., Metzger M. R., Moore C. B., 2001, ApJ, 546, 681
- Tormen G., 1997, MNRAS, 290, 411
- Trujillo I., Burkert A., Bell E. F., 2004, ApJ, 600, L39
- van den Bosch F. C., Yang X., Mo H. J., Norberg P., 2005, MNRAS, 356, 1233
- Wechsler R. H., Bullock J. S., Primack J. R., Kravtsov A. V., Dekel A., 2002, ApJ, 568, 52
- Zaritsky D., Gonzalez A. H., Zabludoff A. I., 2004, ApJ, 613, L93
- Zentner A. R., Bullock J. S., 2003, ApJ, 598, 49
- Zentner A. R., Berlind A. A., Bullock J. S., Kravtsov A. V., Wechsler R. H., 2005, ApJ, 624, 505
- Zhang B., Wyse R. F. G., Stiavelli M., Silk J., 2002, MNRAS, 332, 647